



Título artículo / Títol article: Zinc blende versus wurtzite ZnS nanoparticles: control of the phase and optical properties by tetrabutylammonium hydroxide

Autores / Autors F. A. La Porta,
J. Andrés,
M. S. Li,
J. R. Sambrano,
J. A. Varela
E. Longo

Revista: Phys. Chem. Chem. Phys., 2014, 16, 20127--20137

Versión / Versió: Post-print

Cita bibliográfica / Cita bibliogràfica (ISO 690): Phys. Chem. Chem. Phys., 2014, 16, 20127

url Repositori UJI: <http://hdl.handle.net/10234/126925>

Zinc blende versus wurtzite ZnS nanoparticles: control of the phase and optical properties by tetrabutylammonium hydroxide

F. A. La Porta,^{*ab} J. Andrés,^b M. S. Li,^c J. R. Sambrano,^d J. A. Varela^a and E. Longo^a

Cite this: DOI: 10.1039/c4cp02611j

Received 12th June 2014,
Accepted 1st August 2014

DOI: 10.1039/c4cp02611j

www.rsc.org/pccp

The influence of tetrabutylammonium hydroxide on the phase composition (cubic zinc blende versus hexagonal wurtzite) of ZnS nanoparticles was studied. The ZnS nanoparticles were prepared by a microwave-assisted solvothermal method, and the phase structure and optical properties along with the growth process of ZnS nanoparticles were studied. We report XRD, FE-SEM, EDXS, UV-vis and PL measurements, and first-principles calculations based on TDDFT methods in order to investigate the structural and electronic properties and the growth mechanism of ZnS nanostructures. The effects as well as the merits of microwave heating on the process and characteristics of the obtained ZnS nanostructures and their performance are reported.

1. Introduction

Increased interest in zinc sulfide (ZnS) nanomaterials has arisen mainly due to their applications in different technological fields such as optoelectronic luminescent devices and photovoltaic cells.^{1–5} The synthesis of ZnS nanocrystals with tunable size and phase not only provides alternative variables in tailoring the physical properties of this semiconductor material, but is also vital to develop them as building blocks in constructing the future nanoscale optoelectronic devices using the so-called “bottom-up” approach whereby atoms and molecules self-organize into nano-sized crystals or more complex molecular assemblies.^{6,7} ZnS can adopt three phases: cubic zinc blende, hexagonal wurtzite or the rarely observed cubic rock salt.⁸ The cubic zinc blende structure of ZnS is the most stable form in the bulk which transforms into a hexagonal wurtzite structure at 1020 °C and melts at 1650 °C and both ZnS polymorphs have industrial applications.^{9,10} In both cubic and hexagonal structures, Zn and S atoms are tetrahedrally bonded where the only difference is in the stacking sequence of atomic layers. Nevertheless, with decreasing particle size, the relative stability of two phases changes and low-temperature synthesis of small wurtzite

ZnS nanoparticles have been reported,^{11–14} and very recently, Kulkarni *et al.*¹⁵ reported the ethylenediamine-mediated wurtzite phase formation in ZnS. Controlled fabrication of nanoparticles with different phases is desirable and necessary, which is however still a great challenge.

The kinetics of crystal growth strongly depend on the structure of the material, the properties of the solution, and the nature of the interface between the crystals and the surrounding solution.^{16–18} In particular, the size dependence of the solid–solid phase transition temperature of ZnS nanoparticles has been the subject of intensive study,^{11,19,20} but harnessing the thermodynamic performance of the nanoparticles in a controllable way remains a complicated matter. Phase control in the growth of ZnS crystals is important, because each phase has unique physical properties, for instance, the different phases show different lattice vibration properties and nonlinear optical coefficients.^{21,22}

As the current research moves toward nanoscale phenomena and technology, the exploration of facile and economic methods for the synthesis of ZnS nanostructures has been of great interest. However, the crystal structure of the nanoparticles strongly depends on the synthesis conditions. Zhang *et al.*²³ by combining molecular dynamics simulations and experimental measurements suggested that wurtzite particles with size smaller than about 7 nm, *in vacuo*, are more stable than zinc blende *in vacuo* at room temperature, however, lowering of the temperature of the zinc blende to wurtzite structure transition is possible for nanosized ZnS using modifiers, and these authors also have reported water-driven structure transformation in nanoparticles at room temperature. Within this framework, achievement of suitable control of the phase transition

^a Instituto de Química, UNESP, PO Box 355, 14801-970, Araraquara, SP, Brazil.
E-mail: felipe_laporta@yahoo.com.br; Fax: +55 16 3301 9691;
Tel: +55 16 3301 9892

^b Department of Analytical and Physical Chemistry, Univ Jaume I,
Castelló de la Plana, 12071, Spain

^c Departamento de Física, USP, PO Box 369, 13560-970 São Carlos,
São Paulo, Brazil

^d Laboratório de Simulação Molecular, UNESP, PO Box 473, 17033-360 Bauru,
SP, Brazil

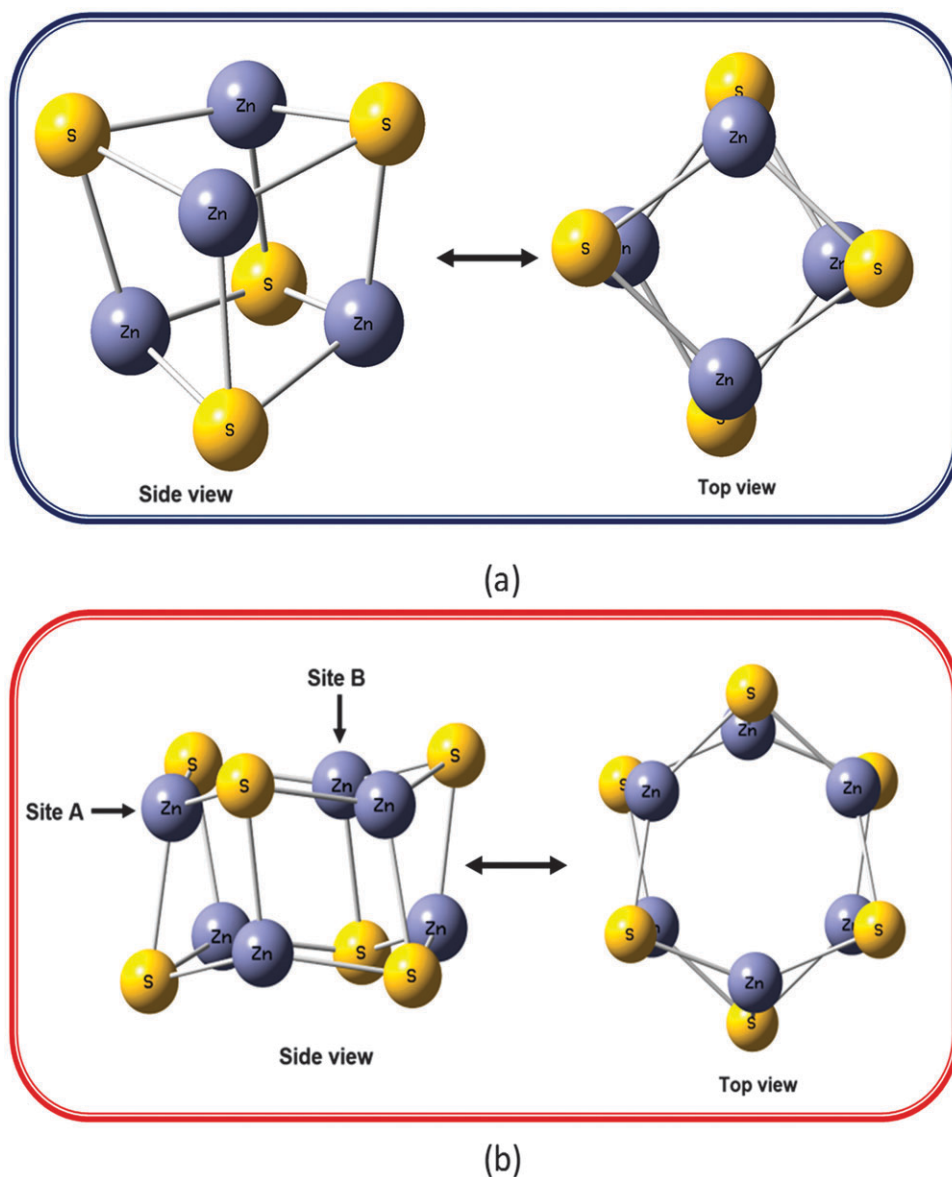
1 behavior of nanometer-sized ZnS materials would represent a
2 significant progress on the way to their full exploitation in
3 different areas of science and engineering.

4 In recent years, well-defined ZnS nanoparticles with various
5 morphologies and structures, including nanotubes, nanorods,
6 nanowires, nanocubes, nanospheres, nanoflowers and
7 nanosheets, have been successfully synthesized and studied
8 using a variety of methods.^{9,24–31} In addition to these techni-
9 ques, the preparation of ZnS *via* solution chemical routes
10 provides a promising option for the large-scale production of
11 this material. Therefore, it is important to develop new envi-
12 ronmentally friendly processing material methods with low cost,
13 and with the possibility of formation of nanoscale materials
14 with phase control and well-defined morphologies. Developing
15 this phase-selective synthesis, in general, is crucial for the

design of ZnS nanocrystals with novel tunable physical proper-
ties which is of great interest in nanotechnology.

The synthesis route of nanoparticles has a major influence on
their size, shape and optical properties. Recently, a microwave-
assisted procedure has been developed into an efficient method
for the fabrication of nanomaterials, and is becoming very attractive
in all areas of synthetic chemistry because it has some advantages
over other synthetic methods,^{32,33} because the application of micro-
wave irradiation in chemical transformations often results in dra-
matic rate accelerations, enhanced yields, cleaner reactions^{32–36} and
improved material quality and size distributions in nanomateri-
als.^{34–40} Some comprehensive reviews on microwave-assisted syn-
theses of nanomaterials have been published.^{37,41}

The mechanism associated with microwave effects in synthesis
are not well understood,^{38,42,43} and this is an open research field.



55 **Fig. 1** Geometry of the ZnS clusters. (a) Zn_4S_4 and (b) Zn_6S_6 clusters have been selected to represent the cubic zinc blende and the hexagonal
wurtzite, respectively.

In such cases, it is certain that quantum chemistry tools are extremely helpful in the rationalization and interpretation of reaction mechanisms at the atomic level, based on the characterization of key intermediates along the reaction pathways.

Here we report a rapid and economical microwave-assisted route for the preparation and phase control of ZnS nanoparticles by a simple microwave-assisted solvothermal (MAS) method and the presence of tetrabutylammonium hydroxide. The formation mechanism and the conditions under which the phase of the synthesized ZnS (wurtzite and zinc blende) is obtained are discussed in detail. The obtained materials were analyzed by X-ray diffraction (XRD), field emission scanning electron microscopy (FE-SEM), energy dispersive X-ray spectroscopy (EDXS), and ultraviolet-visible (UV-vis) and photoluminescence (PL) measurements. Targeting a better understanding of the experimental data, theoretical calculations were carried out by time-dependent density functional theory (TDDFT). In addition, this study gives practical guidance for controlling the phase in MAS growth of ZnS nanostructures, and the effects as well as the merits of microwave heating on the process and characteristics of the obtained ZnS powders are reported.

2. Methodology

2.1 Materials

All reagents were of analytical grade and were used without further purification. ZnS nanostructures were synthesized by the MAS method with or without modifier assistance, in the presence of ethylene glycol (EG) at 140 °C and for short times.

In a typical procedure, 7.34 mmol of zinc acetate are dissolved in 25 mL of EG and heated to 80 °C (solution 1); 7.34 mmol of thiourea are separately dissolved in another 25 mL of EG (solution 2). With vigorous magnetic stirring, solution 1 is then quickly injected into solution 2. In the sequence, the solution was transferred into a Teflon autoclave, which was sealed and placed inside a domestic microwave-solvothermal system (2.45 GHz, maximum power of 800 W). The microwave-assisted solvothermal process was performed at 140 °C for 10 min. The resulting precipitate was washed with deionized water and ethanol to remove byproducts possibly remaining in the final product and the precipitates were finally collected and dried at 70 °C overnight. The synthesis was also performed with the assistance of a modifier. For this we conducted the same procedure described above with the addition of 15.44 mmol of tetrabutylammonium hydroxide (40%) in solution 1.

2.2 Characterization

The obtained powders were structurally characterized by XRD using a Rigaku-DMax/2500PC with Cu K α radiation ($\lambda = 1.5406 \text{ \AA}$) in the 2θ range from 10° to 75° with $0.02^\circ \text{ min}^{-1}$. The phase analysis by the Rietveld method⁴⁴ was carried out using the General Structure Analysis System (GSAS) software.⁴⁵

The morphologies of ZnS powder were observed by FE-SEM using a FEG-VP JEOL. The compositional analysis as well as the mapping of the elements in the analyzed samples was performed by means of energy dispersive X-ray spectroscopy

(EDXS). Optical properties were analyzed by means of UV-vis absorption spectroscopy using a Cary 5G spectrophotometer (Varian, USA) in diffuse reflection mode.

2.3 Computational details and model systems

All calculations were carried out using the Gaussian 09 program package.⁴⁶ The structures of the reactants, intermediates, and products formed during the growth process for the model systems have been fully optimized by TDDFT using the B3LYP functional^{47,48} employing the standard all-electron 6-311+G(d,p) basis set to describe the atoms. No imaginary frequencies were found for the optimized geometries. The solvent effect was evaluated with utilization of a polarized continuum model (PCM),^{49,50} using a dielectric constant of 41.4 to simulate the EG.

Two model systems, Zn₄S₄ and Zn₆S₆ clusters, have been selected to represent the cubic zinc blende and the hexagonal wurtzite, respectively (see Fig. 1). For the Zn₄S₄ and Zn₆S₆ clusters, the local structure, excitation energy and oscillator strength for electronic transitions from the ground to excited states have been obtained by means of TDDFT calculations using a 6-311+G(d,p) basis set. Molecular orbital (MO) pictures were prepared using the Gaussian View 2.1 package⁴⁶ using a

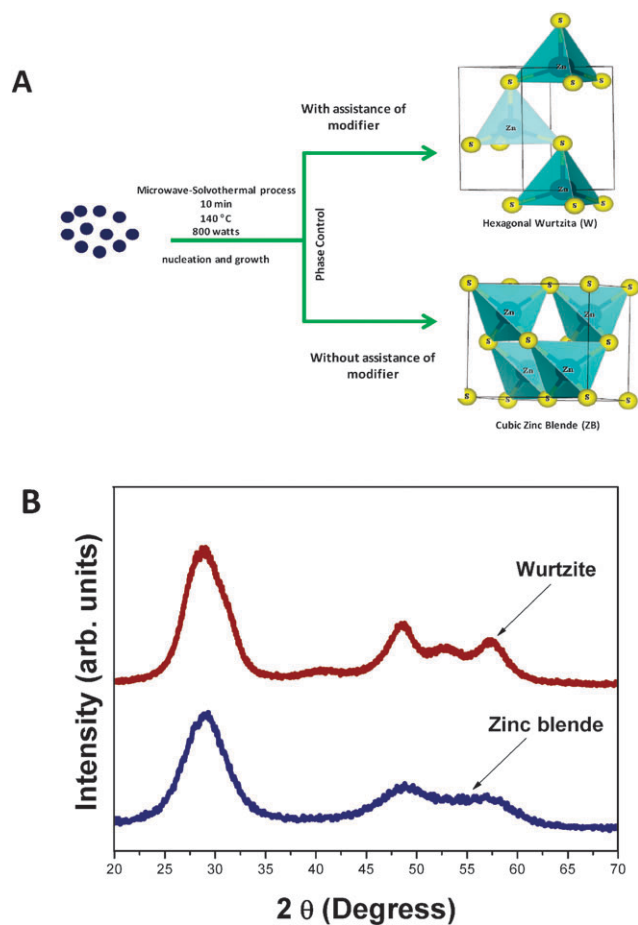


Fig. 2 (A) A schematic representation of the synthesis of ZnS nanostructures (cubic versus hexagonal) by means of the microwave-assisted solvothermal method, in which phase control is provided by the modifier (tetrabutylammonium hydroxide). (B) XRD patterns of ZnS nanostructures at 140 °C.

1 contour value of 0.030 and projected density of states (DOS) was analyzed using GaussSum.⁵¹

To understand the role of the modifier in the synthesis, *i.e.* tetrabutylammonium hydroxide, the interaction energy with the surface of both Zn₄S₄ and Zn₆S₆ clusters has been obtained, following eqn (1):

$$\Delta E_{\text{inter}} = E_{A/B} - E_A - E_B \quad (1)$$

10 where ΔE_{inter} is the interaction energy, $E_{A/B}$ is the total energy calculated for the modifier molecule adsorbed on the surface of Zn₄S₄ or Zn₆S₆ clusters, E_A is the energy of the modifier molecule and E_B is the energy of the clusters.

15 3. Results and discussion

Fig. 2 depicts the XRD patterns, showing that the samples processed with the MAS method are highly crystalline, pure and ordered in a long range. All diffraction peaks of ZnS nanoparticles can be indexed to the hexagonal structure or cubic structure in agreement with the respective Joint Committee on Powder Diffraction Standard

25 **Table 1** Crystallite size and reaction yield of ZnS nanostructures with or without any modifier assistance at 140 °C

Structures	XRD particle size (Å)	Reaction yield (%)
W	20.20	91.59
ZB	17.72	67.88

(JCPDS) cards 36–1450 and 80–20.^{52,53} No other diffraction peaks are found, which indicates that the products are pure ZnS.

The diffraction peaks are significantly broadened because of the very small crystallite size. The mean crystallite size, T , was calculated from the Scherrer equation (eqn (2)):⁵⁴

$$T = \frac{0.9\lambda}{\beta \cos \theta} \quad (2)$$

where λ is the K $_{\alpha}$ radiation; θ is the Bragg diffraction angle; and β is the width of the peak at half the maximum intensity in radians (Table 1). The strain and grain size of both samples were calculated by the Williamson–Hall (W–H) method, according to the following equation (eqn (3)).⁵⁵ In particular, the W–H analysis is a simplified integral breadth method where strain-induced broadening arises from crystal imperfections and distortion in the lattice.^{56–58} Thus, the full width at half maximum (FWHM) may be expressed in terms of strain (ε) which is estimated from the slope of the line and the crystallite size (T) from the intersection with the vertical axis, and other parameters have the same meaning as in eqn (2). The W–H plot of ZnS nanoparticles obtained by the MAS method is shown in Fig. 3(b and d).

$$\frac{\beta \cos \theta}{\lambda} = \frac{0.9}{T} + \frac{\varepsilon \sin \theta}{\lambda} \quad (3)$$

In order to prove that compounds obtained by the MAS method are pure and feature a single-phase the Rietveld refinement method was employed in this study, with the

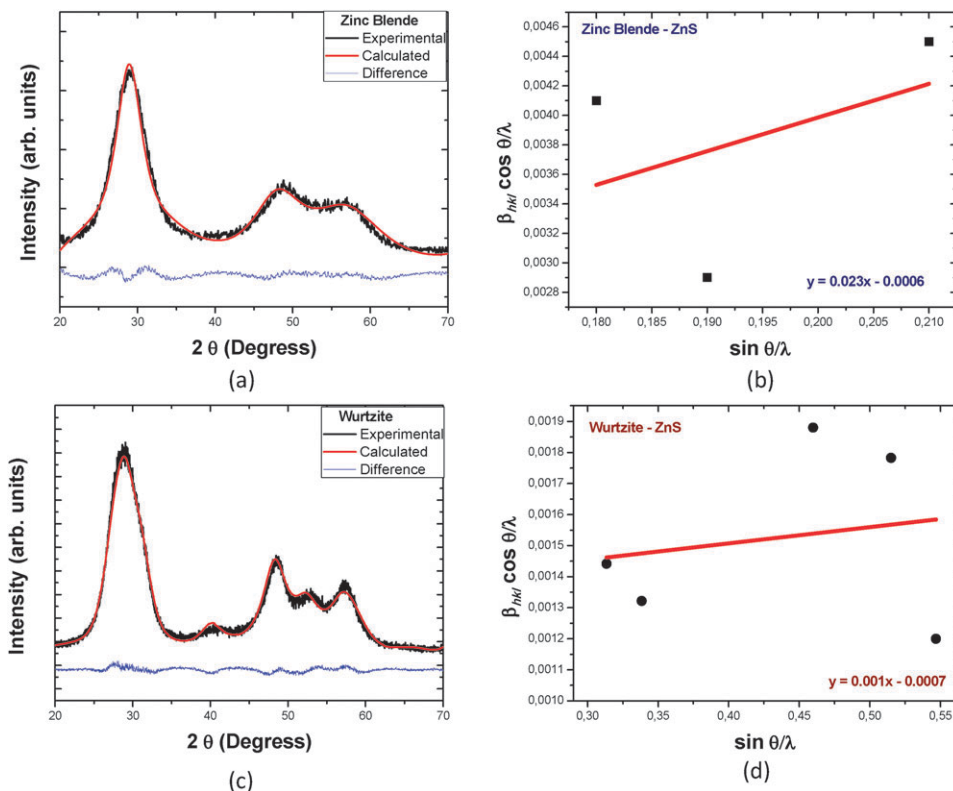


Fig. 3 Williamson–Hall analysis and Rietveld refinement plot of ZnS nanoparticles processed by MAS at 140 °C: (a and b) zinc blende and (c and d) wurtzite.

1 **Table 2** Rietveld refinement results for the ZnS nanoparticles

Lattice parameter	ICSD ^a		MAS	
	Zinc blende	Wurtzite	Zinc blende	Wurtzite
5 a (Å)	5.32	3.82	5.48	3.80
c (Å)	—	6.26	—	6.24
R_{wp} (%)	—	—	10.88	6.23
R_p (%)	—	—	7.71	5.24
R_b (%)	—	—	0.561	0.303
χ^2	—	—	0.897	2.679

10 ^a ICSD no. 41 985 and 67 453, respectively.⁶⁰

specific objective of analyzing and understanding whether there are differences in the structural arrangements and determining the size of the particles of ZnS nanoparticles obtained by the MAS method (see Fig. 3(a and c)).

In Rietveld analysis, fitting parameters (R_{wp} , R_p , R_{exp} and χ^2) indicate good agreement between refined and observed XRD patterns for the samples obtained by the MAS method (see Table 2). These phases corresponding to the different

polymorphs of ZnS can be clearly identified in this case, it was noted that the lattice parameters and unit cell volumes obtained for both zinc blende and wurtzite of the ZnS structures are very close to those published in the literature.^{58,59}

However, some variations in the atomic positions related to sulfur atoms were observed while zinc atoms have fixed atomic positions. These results indicate certain degree of disorder for the samples obtained by the MAS method, especially the sulfur vacancies. We believe these variations in atomic positions of sulfur atoms can lead to the formation types of distortions on [S–Zn–S] bonds and consequently promote different levels of distortions on the [ZnS₄] and/or [ZnS₃] clusters in the lattice of ZnS.

Our results clearly correspond to two different growth rates for two different directions, implying an irregular spherical-like particle shape promoting a simple way for phase control of ZnS nanoparticles during processing under the MAS conditions; on the other hand, the reaction yields much more hexagonal phase than the cubic phase. These results indicate that the crystal

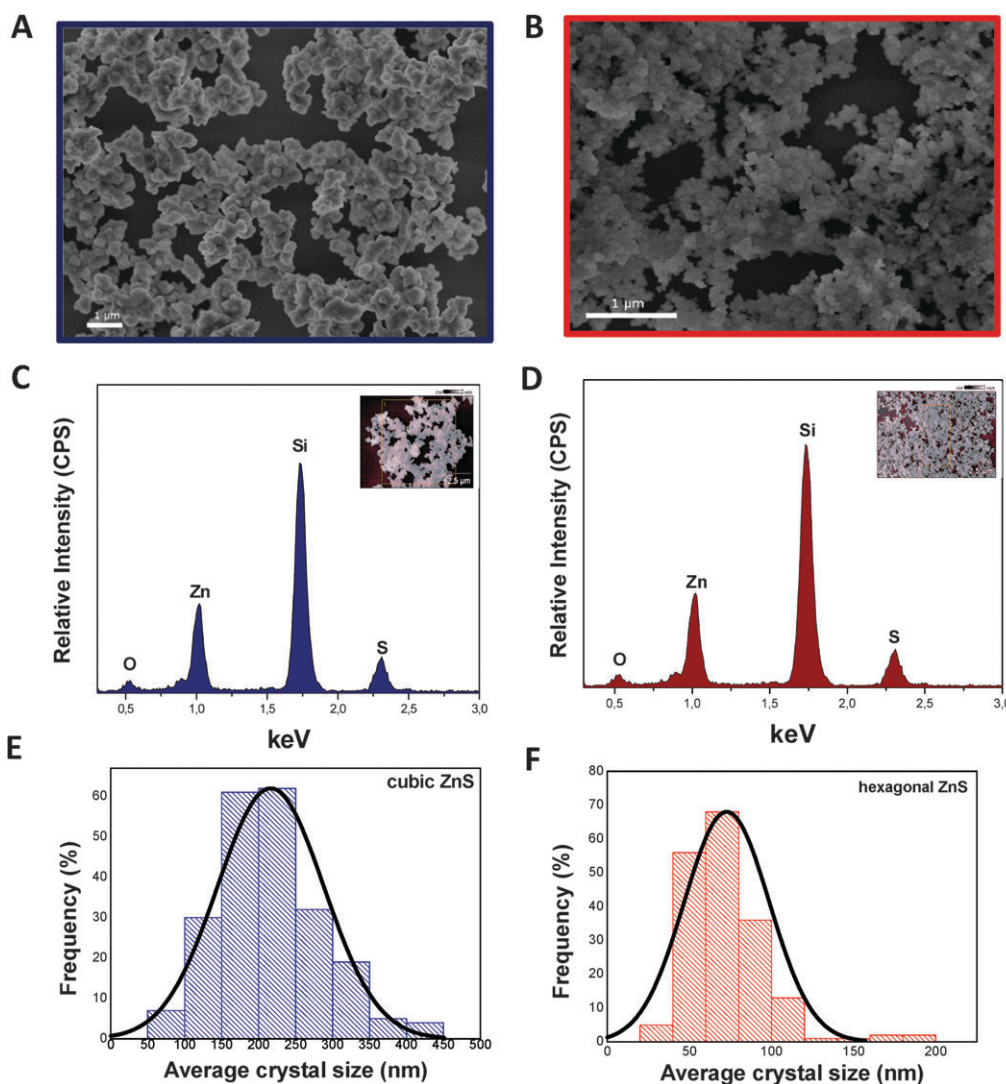


Fig. 4 FEG-SEM images, EDS patterns and particle size distribution of (left) cubic and (right) hexagonal ZnS nanostructures.

1 phase of ZnS prepared by MAS synthesis can be controlled by
 2 adjusting experimental parameters mediated by the presence of
 3 tetrabutylammonium hydroxide (see Fig. 2).

4 The FE-SEM micrographs in Fig. 4 illustrate the influence of
 5 the different preparation conditions on the morphology and size
 6 distribution of the prepared samples. FE-SEM images show that
 7 the synthesis route produces quite similar ZnS crystalline
 8 agglomerate nanoparticles as can be observed on the ZnS particle
 9 facets, as shown in Fig. 4(A and B). The interface characteristics
 10 and growth are strongly driven by the chemistry of the surface,
 11 which in turn contributes to the phase stability.^{17,61–63}

12 The microwave process leads to rapid formation of a high
 13 density of nucleation sites and the growth of the ZnS nano-
 14 particles. These nanocrystals have a strongly polarized surface,
 15 because of a high concentration of short and intermediate-range
 16 defects. In previous studies,⁹ we suggested that the growth of ZnS
 17 obtained by MAS can be described *via* a nucleation–dissolution–
 18 recrystallization mechanism, and this mechanism is responsible
 19 for the fast nucleation of the ZnS small particles which aggregate
 20 into a spherical morphology to minimize their surface energy. In
 21 general, the nucleation–dissolution–recrystallization mechanism
 22 occurs using the MAS method,^{9,38,40,64} which is considered highly
 23 sensitive to relative rates of amorphous solid particle dissolution
 24 and nucleation of the crystalline phase.^{17,38,64–68} As a conse-
 25 quence, this mechanism involves the formation of a high concen-
 26 tration of aggregated nanoparticles with predominant growth
 27 controlled by the coalescence process.³⁹ EDXS reveals that the
 28 products contain Zn and S which are in excellent agreement with
 29 the stoichiometry of ZnS, indicating the purity of the sample
 30 processed by the MAS method. The EDXS spectra are also very
 31 similar to the spectrum of ZnS published by Ludi *et al.*⁶⁹

32 In recent years, considerable effort has been devoted to the
 33 synthesis of nanocrystals prepared by a solvothermal process
 34 using various modifiers to control and induce the growth of
 35 nanocrystals.^{39,70–78} The modifier plays a different role in each
 36 type of synthesis, and their effects are not completely under-
 37 stood. The use of a modifier in the chemical synthesis of
 38 nanomaterials has been employed to obtain new shapes with
 39 different sizes, which promotes the formation of materials with
 40 different chemical behaviour.^{76–78}

41 According to Lamer and Dinegar,⁷⁹ the precursor conversion
 42 reactions that limit the crystallization determine the temporal
 43 evolution of monomer concentration as well as the steady state
 44 supersaturation during the growth phase. In our case, the
 45 $[\text{Zn}(\text{SH})_4]^{2-}$ complex in solution can be considered as the growth
 46 unit for the ZnS nanostructures.^{80–82} Therefore, we propose a
 47 growth process of ZnS nanostructures as shown in Fig. 5, and to
 48 further understand the phase control, cubic zinc blende *vs.*
 49 hexagonal wurtzite, we use the Zn_4S_4 and Zn_6S_6 clusters as model
 50 systems (see Fig. 1). These clusters serve as a base for the growth
 51 of larger crystals, and have been experimentally characterized by
 52 mass spectrometry.⁸³ The Zn–S distances calculated are 2.38 and
 53 2.32/2.42 Å for the cubic zinc blende Zn_4S_4 and hexagonal wurtzite
 54 Zn_6S_6 clusters, respectively, which are in good agreement with
 55 other theoretical studies.^{83–88} It is important to note that the
 56 experimental values of the lattice parameters reported for the bulk

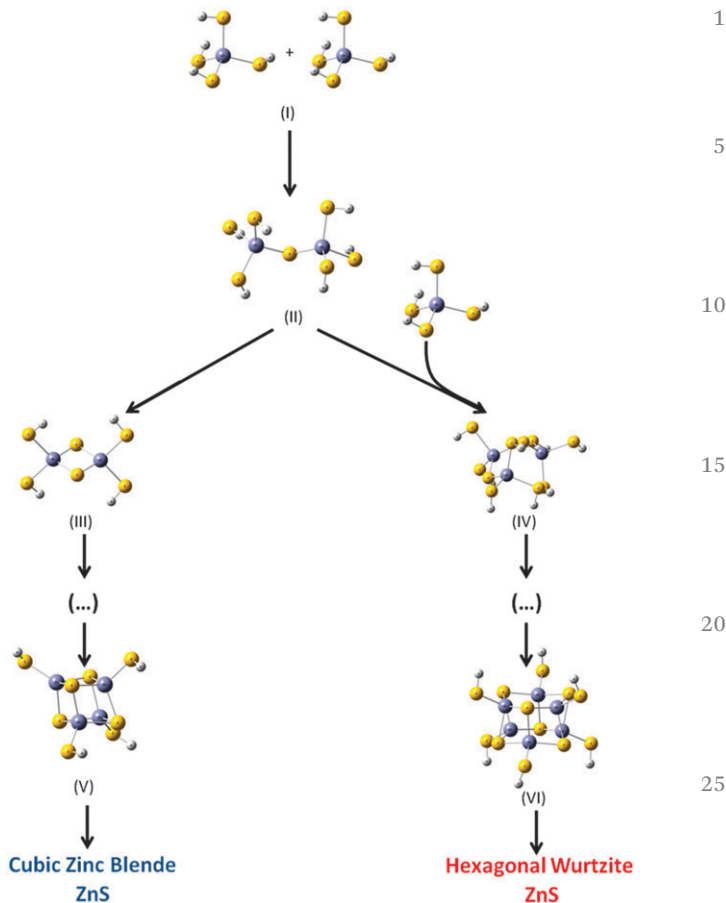


Fig. 5 Proposed intermediates along the reaction pathways to obtain cubic and hexagonal ZnS nanostructures.

ZnS structures exhibit Zn–S bonding distances that are quite similar for wurtzite and zinc blende (~ 2.34 Å), due to the great similarity in the local coordination of the tetrahedral $[\text{ZnS}_4]$ cluster in the lattice.⁸⁹

The theoretical infrared- and Raman-active modes for the Zn_4S_4 and Zn_6S_6 clusters are shown in Fig. 6. An analysis of the results yields two and five active infrared lines, while four and seven active lines in the Raman spectra are found for the Zn_4S_4 and Zn_6S_6 clusters, respectively.

The condensation of these complexes occurs through a mechanism of nucleophilic substitution, in which two original zinc complexes or monomers are found in the solution and react to form a dimer, with elimination of H_2S and form sulfur bridges (intermediate II) $[\text{Zn–S–Zn}]$ with stronger chemical bonds. From this intermediate II, there are two possible reaction pathways: (i) the intramolecular cyclic rearrangement of this dimer to form a cyclic structure, intermediate III, or (ii) the formation of a trimer, intermediate IV. This second step can be associated with the phase control along the growth process of ZnS nanocrystals. We have estimated differences in Gibbs free energies to study the reaction mechanism. This, however, is a crude approximation because medium effects are not taken into account. An analysis of the results shows that the reaction pathway for the formation at the nanoscale of ZnS suggests that

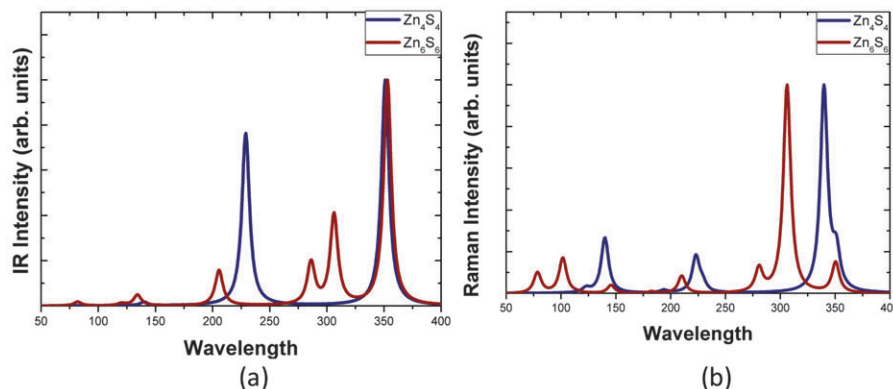


Fig. 6 Theoretical vibrational modes, (a) infrared and (b) Raman, obtained at the B3LYP/6-31+G calculation level for Zn_4S_4 and Zn_6S_6 cluster models.

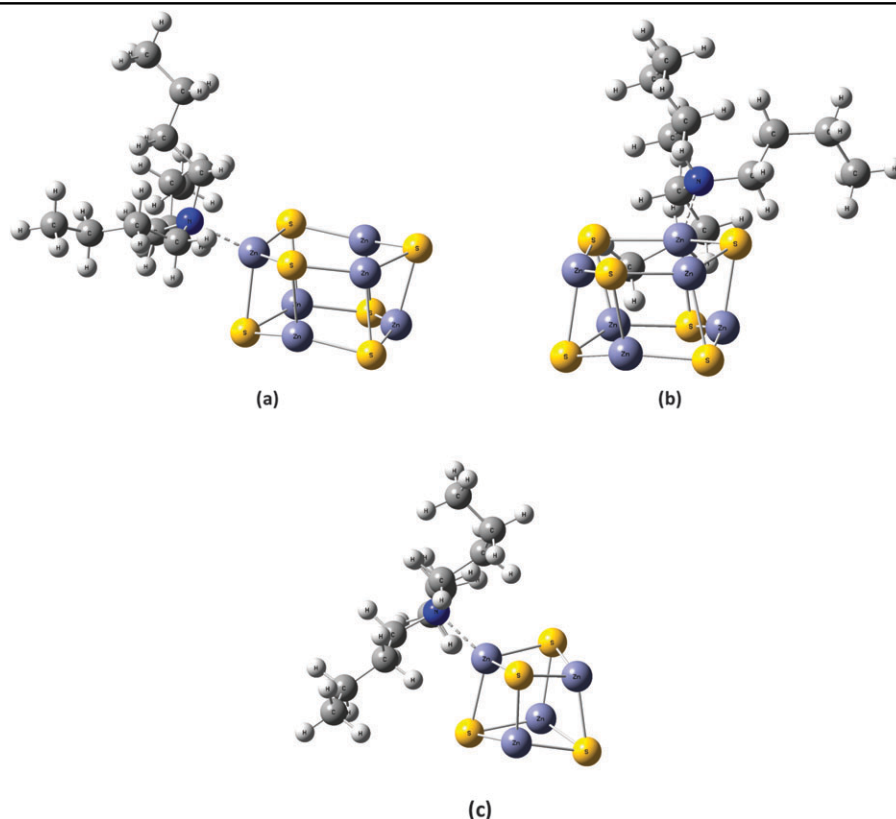
the formation of the trimer (intermediate III) is more favorable energetically by about $156.59 \text{ kcal mol}^{-1}$ relative to formation of a cyclic structure (intermediate IV). Thus, based on these results we can show that the hexagonal wurtzite phase is more favorable energetically with respect to cubic zinc blende from a thermodynamic point of view on the nanoscale.

With respect to structures shown in Fig. 1, the Zn_4S_4 cluster has only one type of Zn atom, while the hexagonal phase (Zn_6S_6

cluster) contains two different Zn atoms in this cluster that can be thought of as the unit cell of a wurtzite structure. More recently, a benchmark data set using DFT and TDDFT of geometrical parameters, vibrational normal modes, and low-lying excitation energies for these clusters has been reported by Azpiroz *et al.*⁸⁸

The calculated values of the interaction energy of the modifier molecule, tetrabutylammonium hydroxide, on the surface

Table 3 Selected geometrical parameters and values of the interaction energy (ΔE_{inter}) between the modifier molecule and the different ZnS cluster models



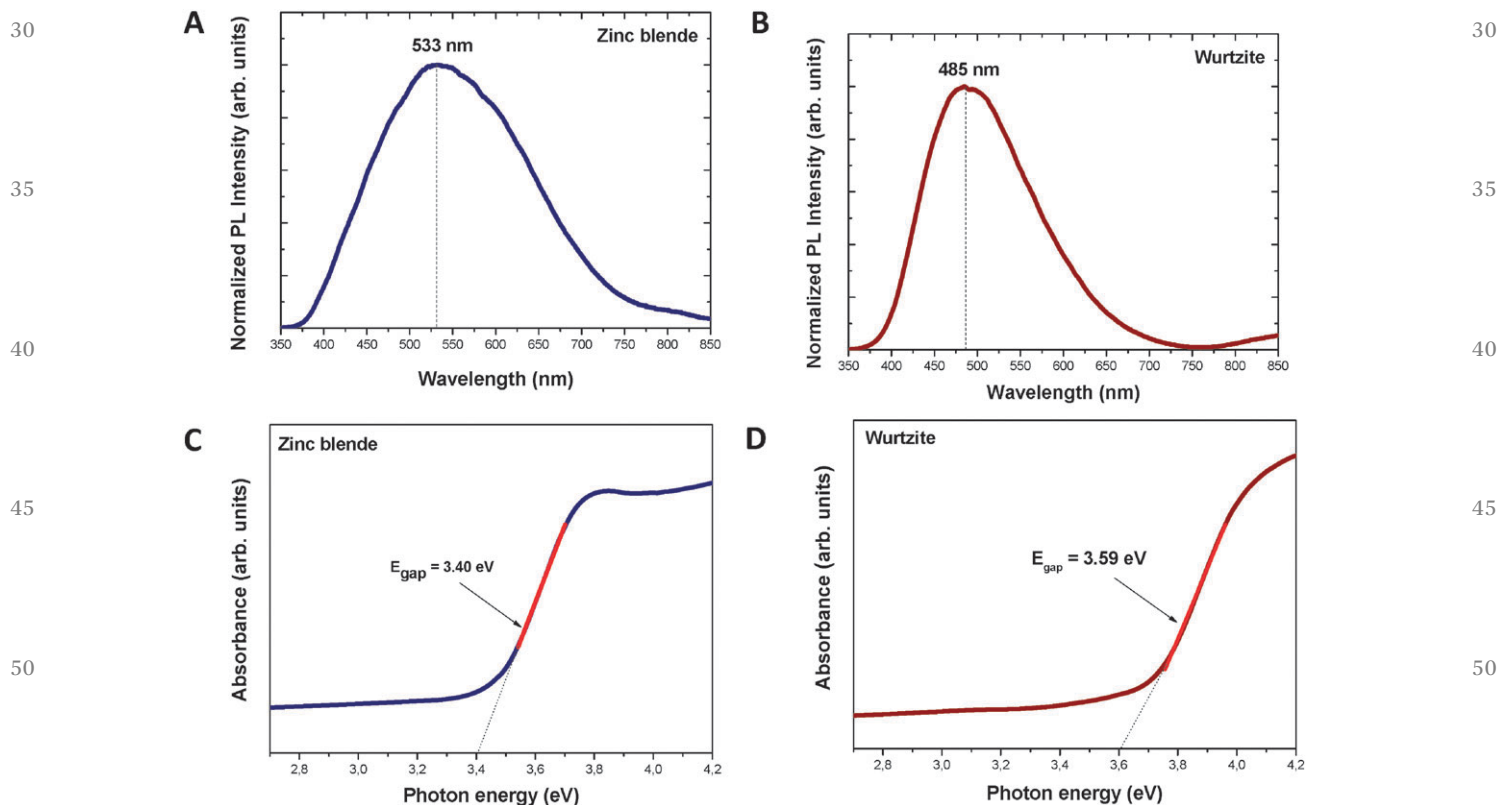
Model	Bond length _{Zn-N} (Å)	Angle [N-Zn-S] (°)	ΔE_{inter} (kcal mol ⁻¹)
Zn ₆ S ₆ site A	2.18	114.03	-87.27
Zn ₆ S ₆ site B	2.15	110.47	-94.23
Zn ₄ S ₄	2.10	117.04	-30.87

1 of Zn_6S_6 (with the active sites A and B) and Zn_4S_4 clusters and the corresponding optimized geometries are given in Table 3. An analysis of the results shows that the value of the interaction energies of the modifier are energetically favorable, at the A
5 (−87.27 kcal mol^{−1}) and B (−94.23 kcal mol^{−1}) sites which are more favorable in the Zn_6S_6 cluster than in the Zn_4S_4 cluster (−30.87 kcal mol^{−1}). In particular, theoretical calculations on the relative stability of both phases of the bulk ZnS have been
10 previously studied by Yeh *et al.*⁹⁰ This result can explain that the tetrabutylammonium hydroxide modifier favors the formation of the hexagonal wurtzite phase with respect to the cubic phase.

According to the literature,^{9,39} ZnS exhibits an optical absorption spectrum governed by direct electronic transitions. UV-Vis diffuse reflectance spectroscopy was used to determine the band gap of these materials in order to better understand the differences in ZnS nanostructures (see Fig. 7(A and B)). The Kubelka–Munk method based on diffuse reflectance spectroscopy was employed to determine the band gap of these materials.⁹ UV-vis absorption measurements illustrate a variation in the optical band gap values from 3.40 to 3.59 eV for ZnS nanoparticles, for the zinc blende structure and wurtzite structure, respectively. After the electronic absorption process, electrons located in the maximum-energy states in the valence band revert to minimum-energy states in the conduction band under the same point in the Brillouin zone.³⁹ In particular, the band gap values obtained for the samples are much lower than the expected band gap values of 3.68 eV for the zinc blende and
25 3.77 eV for the wurtzite, respectively, for the bulk ZnS reported by Fang *et al.*² The exponential optical absorption edge and the optical band gap energy are controlled by the degree of structural disorder in the lattice.^{9,39,40} The decrease in the band gap value can be attributed to defects and local bond distortion as well as
5 intrinsic surface states and interfaces which yield localized electronic levels within the forbidden band gap, due to electron transitions from the valence band to the conduction band.

Fig. 7(C and D) show PL evolution of ZnS samples synthesized by a MAS method with or without any modifier assistance at 140 °C. The PL spectra of ZnS samples present a broad band covering the visible electromagnetic spectra in the range from 400 to 800 nm, with maximum emission at 485 and 530 nm, for the hexagonal structures and cubic structures respectively, when excited by a 350.7 nm laser line. This behavior is due to changes in the shape, crystal size, structure and orientation of ZnS crystals. The emission band profile is typical of a multiphonon process; *i.e.*, a system where relaxation occurs by several paths involving the participation of numerous states within the band gap of the material.^{9,39} In this scenario, we have investigated the electronic structure of the cubic zinc blende Zn_4S_4 and hexagonal wurtzite Zn_6S_6 clusters using the frontier molecular orbitals obtained from TDDFT calculations.

Fig. 8 shows the shape of molecular orbitals calculated for the Zn_4S_4 and Zn_6S_6 clusters. The HOMO–LUMO gaps calculated and experimental values in parentheses are 3.16 (3.40) and 3.88 (3.59) eV for the Zn_4S_4 and Zn_6S_6 clusters, respectively,^{83–88} while the values of the energy of first ionization potentials (IPs), calculated in



55 **Q5** Fig. 7 Optical properties of both cubic and hexagonal ZnS nanostructures: (A and B) normalized PL spectra at room temperature, (C and D) UV-vis spectra and (E) schematic representation of the optical properties involving fundamental and excited electronic states.

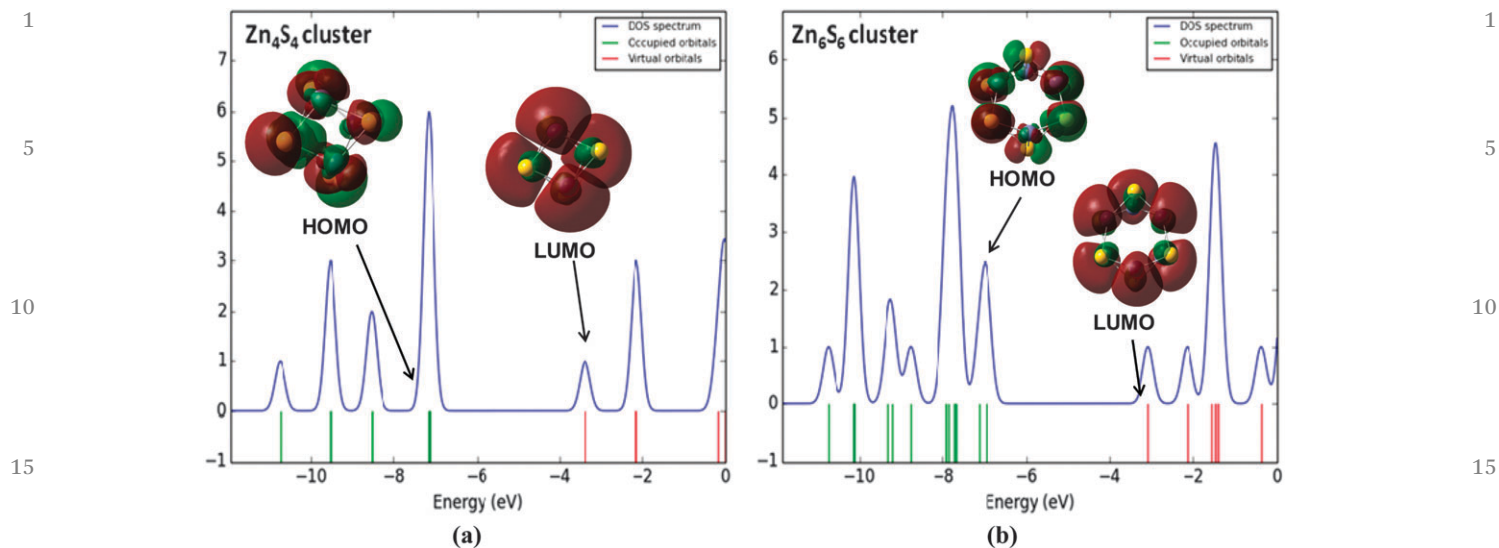
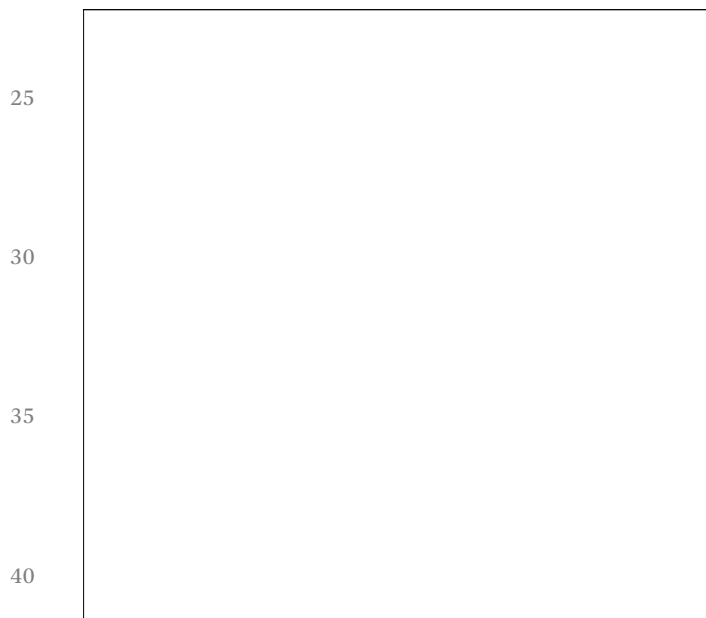


Fig. 8 Representation of the frontier molecular orbitals and the projected DOS obtained at the TDDFT calculation level: (a) the cubic zinc blende Zn_4S_4 cluster and (b) the hexagonal wurtzite Zn_6S_6 cluster.

20

20



Q6 Fig. 9 Optimized structures involving the interaction of a modifier molecule (tetrabutylammonium hydroxide) with ZnS clusters at different active sites of Zn atoms. (a) Zn_6S_6 site A, (b) Zn_6S_6 site B and (c) Zn_4S_4 clusters.

45

the framework of Koopmans' theorem⁹¹ are 7.15 and 6.95 eV for the Zn_4S_4 and Zn_6S_6 clusters, respectively. An analysis of the DOS for the cubic Zn_4S_4 and hexagonal Zn_6S_6 clusters shows that the HOMO orbital consists mainly of S 3p orbitals whereas the LUMO is composed of Zn 4sp hybrid orbitals (see Fig. 8).

4. Conclusions

55 In summary, we have demonstrated phase control, mediated by the presence of tetrabutylammonium hydroxide, in the growth

of ZnS crystals by using a cost effective MAS method, and a very moderate temperature (140 °C) and a very fast reaction time are sufficient to produce nanostructures with a good degree of crystallinity. XRD, FE-SEM, EDXS measurements and theoretical calculations were extensively employed to investigate structural and surface chemical compositions along the growth process of the synthesized nanostructures. Our results strongly suggest that the crystal phase of the prepared ZnS can be controlled by a modifier, *i.e.* tetrabutylammonium hydroxide and a new route has opened up for constructing novel nanostructures, which gives a better understanding of the control of ZnS nanostructures and their optical behaviour at the atomic-level. This finding offers new possibilities and shows that theory can be a suitable partner with experiments in developing and rationalizing these properties at the atomic level which is very important for progress in nanotechnology.

Acknowledgements

The authors gratefully acknowledge the support from the Brazilian agencies FAPESP, CNPq and CAPES. J.A. also acknowledges Generalitat Valenciana for Prometeo/2009/053 project, Ministerio de Economía y Competitividad (Spain) under project CTQ2012-36253-C03-02, and Programa de Cooperación Científica con Iberoamerica (Brasil), Ministerio de Educación (PHB2009-0065-PC). Special appreciation is extended to Dr D. P. Volanti for the development of the MAS method.

Notes and references

- 1 Y. C. Cao and J. Wang, *J. Am. Chem. Soc.*, 2004, **126**, 14336.
- 2 X. Fang, T. Zhai, U. K. Gautam, L. Li, L. Wu, Y. Bando and D. Golberg, *Prog. Mater. Sci.*, 2011, **56**, 175.
- 3 X. Wang, J. Shi, Z. Feng, M. Li and C. Li, *Phys. Chem. Chem. Phys.*, 2011, **13**, 4715.

- 1 4 A. K. Kole, C. S. Tiwary and P. Kumbhakar, *CrystEngComm*, 2013, **15**, 5515.
- 5 F.-J. Fan, L. Wu and S.-H. Yu, *Energy Environ. Sci.*, 2014, **7**, 190.
- 5 6 Y. G. Zhang, G. Y. Wang, X. Y. Hu, Q. F. Shi, T. Qiao and Y. Yang, *J. Cryst. Growth*, 2005, **284**, 554.
- 7 N. S. N. Jothi and P. Sagayaraj, *Arch. Appl. Sci. Res.*, 2012, **4**, 1079.
- 8 F. A. La Porta, L. Gracia, J. Andrés, J. R. Sambrano, J. A. Varela and E. Longo, *J. Am. Ceram. Soc.*, 2014, in press.
- 9 F. A. La Porta, M. M. Ferrer, Y. V. B. Santana, C. W. Raubach, V. M. Longo, J. R. Sambrano, E. Longo, J. Andrés, M. S. Li and J. A. Varela, *J. Alloys Compd.*, 2013, **556**, 153.
- 10 P. K. Giri, D. K. Goswami and A. Perumal, *Advanced Nanomaterials and Nanotechnology*, Springer-Verlag, Berlin, Heidelberg, 2013, p. 66.
- 15 11 Y. Zhao, Y. Zhang, H. Zhu, G. C. Hadjipanayis and J. Q. Xiao, *J. Am. Chem. Soc.*, 2004, **126**, 6874.
- 12 F. Huang and J. F. Banfield, *J. Am. Chem. Soc.*, 2005, **127**, 4523.
- 20 13 J. Q. Sun, X. P. Shen, K. M. Chen, Q. Liu and W. Liu, *Solid State Commun.*, 2008, **147**, 501.
- 14 H. Tong, Y. J. Zhu, L. X. Yang, L. Li, L. Zhang, J. Chang, L. Q. An and S. W. Wang, *J. Phys. Chem. C*, 2007, **111**, 3893.
- 25 15 S. A. Acharya, N. Maheshwari, L. Tatikondewar, A. Kshirsagar and S. K. Kulkarni, *Cryst. Growth Des.*, 2013, **13**, 1369.
- 16 J. Zhang, Z. Lin, Y. Lan, G. Ren, D. Chen, F. Huang and M. Hong, *J. Am. Chem. Soc.*, 2006, **128**, 12987.
- 30 17 J. J. De Yoreo and P. G. Vekilov, in *ReViews in Mineralogy and Geochemistry: Biomineralization*, ed. P. M. Dove, J. J. De Yoreo and S. Weiner, Mineralogical Society of America, Washington, DC, 2003, vol. 54, p. 57.
- 18 F. C. Meldrum and H. Cölfen, *Chem. Rev.*, 2008, **108**, 4332.
- 35 19 C. A. Feigl, A. S. Barnard and S. P. Russo, *Phys. Chem. Chem. Phys.*, 2012, **14**, 9871.
- 20 C. A. Feigl, S. P. Russo and A. S. Barnard, *J. Mater. Chem.*, 2010, **20**, 4971.
- 21 O. Brafman and S. S. Mitra, *Phys. Rev.*, 1968, **171**, 931.
- 40 22 Y. Ding, X. D. Wang and Z. L. Wang, *Chem. Phys. Lett.*, 2004, **398**, 32.
- 23 H. Zhang, B. Gilbert, F. Hung and J. F. Banfield, *Nature*, 2003, **424**, 1025.
- 24 Y. Chen, Q.-S. Wu and Y.-P. Ding, *J. Braz. Chem. Soc.*, 2007, **18**, 924.
- 45 25 L. S. Li, N. Pradhan, Y. Wang and X. Peng, *Nano Lett.*, 2004, **4**, 2261.
- 26 J. Joo, H. B. Na, T. Yu, J. H. Yu, Y. W. Kim, F. Wu, J. Z. Zhang and T. Hyeon, *J. Am. Chem. Soc.*, 2003, **125**, 11100.
- 50 27 A. K. Kole, C. S. Tiwary and P. Kumbhakar, *J. Mater. Chem. C*, 2014, **2**, 4338.
- 28 J. Kennedy, P. P. Murmu, P. S. Gupta, D. A. Carder, S. V. Chong, J. Leveneur and S. Rubanov, *Mater. Sci. Semi-cond. Process.*, 2014, **26**, 561.
- 55 29 C. S. Pathak, M. K. Mandal, D. D. Mishra and V. Agarawala, *J. Adv. Microsc. Res.*, 2013, **8**, 222.
- 30 X. Huang, M.-G. Willinger, H. Fan, Z.-L. Xie, L. Wang, A. Klein-Hoffmann, F. Girgsdies, C.-S. Lee and X.-M. Meng, *Nanoscale*, 2014, in press.
- 31 Y. S. Jang and Y. C. Kang, *Phys. Chem. Chem. Phys.*, 2013, **15**, 16437.
- 5 32 T. N. Glasnov and C. O. Kappe, *Chem. – Eur. J.*, 2011, **17**, 11956.
- 33 H. Katsuki and S. Komarneni, *J. Ceram. Soc. Jpn.*, 2011, **119**, 525.
- 34 H.-Q. Wang and T. Nann, *ACS Nano*, 2009, **3**, 3804.
- 10 35 G. B. Dudley, A. E. Stiegman and M. R. Rosana, *Angew. Chem., Int. Ed.*, 2013, **52**, 7918.
- 36 I. Bilecka and M. Niederberger, *Nanoscale*, 2010, **2**, 1358.
- 37 M. Baghbanzadeh, L. Carbone, P. D. Cozzoli and C. O. Kappe, *Angew. Chem., Int. Ed.*, 2011, **50**, 11312.
- 15 38 T. A. Mulinari, F. A. La Porta, J. Andrés, M. Cilense, J. A. Varela and E. Longo, *CrystEngComm*, 2013, **15**, 7443.
- 39 Y. V. B. Santana, C. W. Raubach, M. M. Ferrer, F. La Porta, J. R. Sambrano, V. M. Longo, E. R. Leite and E. Longo, *J. Appl. Phys.*, 2011, **110**, 123507.
- 20 40 V. M. Longo, L. S. Cavalcante, E. C. Paris, J. C. Sczancoski, P. S. Pizani, M. S. Li, J. Andrés, E. Longo and J. A. Varela, *J. Phys. Chem. C*, 2011, **115**, 5207.
- 41 Y.-J. Zhu and F. Chen, *Chem. Rev.*, 2014, DOI: 10.1021/cr400366s. Q8
- 42 D. Dallinger and C. O. Kappe, *Chem. Rev.*, 2007, **107**, 2563.
- 25 43 L. Pan, X. Liu, Z. Sun and C. Q. Sun, *J. Mater. Chem. A*, 2013, **1**(29), 8299.
- 44 H. M. Rietveld, *J. Appl. Crystallogr.*, 1969, **2**, 65.
- 45 A. C. Larson and R. B. Von Dreele, *General Structure Analysis System (GSAS)*, Los Alamos National Laboratory Report LAUR, 1994, vol. 86, p. 748.
- 30 46 M. Frisch, *et al.*, Gaussian 09, Revision B.01, Gaussian Inc., Wallingford, CT, 2010.
- 47 A. D. Becke, *J. Chem. Phys.*, 1993, **98**, 5648.
- 48 C. Lee, W. Yang and R. G. Parr, *Phys. Rev. B: Condens. Matter Mater. Phys.*, 1988, **37**, 785.
- 35 49 S. Miertus, E. Scrocco and J. E. Tomasi, *J. Chem. Phys.*, 1981, **55**, 117.
- 50 S. Miertus, *Chem. Phys.*, 1982, **65**, 239.
- 51 N. M. O'Boyle, A. L. Tenderholt and K. M. Langner, *J. Comput. Chem.*, 2008, **29**, 839.
- 40 52 JCPDS File No. 36-1450.
- 53 JCPDS File No. 80-20.
- 45 54 A. Guinier, *X-rays diffraction in crystals, imperfect crystals, and amorphous bodies*, W. H. Freeman, San Francisco, USA, 1963.
- 55 C. Suryanarayana and M. G. Norton, *X-ray Diffraction: A Practical Approach*, Springer, New York, 1998.
- 56 R. Kripal, A. K. Gupta, S. K. Mishra, R. K. Srivastava, A. C. Pandey and S. G. Prakash, *Spectrochim. Acta, Part A*, 2010, **76**, 523.
- 50 57 V. D. Mote, Y. Purushotham and B. N. Dole, *J. Theor. Appl. Phys.*, 2012, **6**, 6.
- 58 A. K. Kole and P. Kumbhakar, *Results Phys.*, 2012, **2**, 150.
- 59 G. O. Siqueira, T. Matencio, H. V. da Silva, Y. G. de Souza, J. D. Ardisson, G. M. de Lima and A. O. Porto, *Phys. Chem. Chem. Phys.*, 2013, **15**, 6796.

- 1 60 (a) B. K. Agrawal, P. S. Yadav and S. Agrawal, *Phys. Rev. B: Condens. Matter Mater. Phys.*, 1994, **15**, 14881; (b) E. H. Kisi and M. M. Elcombe, *Acta Crystallogr., Sect. C: Cryst. Struct. Commun.*, 1989, **45**, 1867.
- 5 61 E. R. Leite, T. R. Giraldo, F. M. Pontes, E. Longo, A. Beltrán and J. Andrés, *Appl. Phys. Lett.*, 2003, **83**(8), 1566.
- 62 H. Zheng, R. K. Smith, Y.-W. Jun, C. Kisielowski, U. Dahmen and A. P. Alivisatos, *Science*, 2009, **324**, 1309.
- 63 A. Elsen, S. Festersen, B. Runge, C. T. Koops, B. M. Ocko, 10 M. Deutsch, O. H. Seeck, B. M. Murphy and O. M. Magnussen, *Proc. Natl. Acad. Sci. U. S. A.*, 2013, **110**, 6663.
- 64 Z. J. Luo, H. M. Li, H. M. Shu, K. Wang, J. X. Xia and Y. S. Yan, *Cryst. Growth Des.*, 2008, **8**, 2275.
- 65 R.-Q. Song and H. Cölfen, *Adv. Mater.*, 2010, **22**, 1301.
- 15 66 H. Cölfen and M. Antonietti, *Mesocrystals and Nonclassical Crystallization*, JohnWiley & Sons Ltd, Chichester, UK, 2008.
- 67 L. Zhou and P. O'Brien, *J. Phys. Chem. Lett.*, 2012, **3**, 620.
- 68 H. Cölfen and M. Antonietti, *Angew. Chem., Int. Ed.*, 2005, **44**, 5576.
- 20 69 B. Ludi, I. Olliges-Stadler, M. D. Rossell and M. Niederberger, *Chem. Commun.*, 2011, **47**, 5280.
- 70 M. Rajamathia and R. Seshadri, *Curr. Opin. Solid State Mater. Sci.*, 2002, **6**, 337.
- 71 G. Zou, H. Li, Y. Zhang, K. Xiong and Y. Qian, *Nanotechnology*, 2006, **17**, S313.
- 25 72 T. He, D. Chen, X. Jiao, Y. Xu and Y. Gu, *Langmuir*, 2004, **20**, 8404.
- 73 C. Zhang, Z. Kang, E. Shen, E. Wang, L. Gao, F. Luo, C. Tian, C. Wang and Y. Lan, *J. Phys. Chem. B*, 2006, **110**, 184.
- 30 74 Q. Zhao, L. Hou and R. Huang, *Inorg. Chem. Commun.*, 2003, **6**, 971.
- 75 A. K. Shahi, B. K. Pandey, R. K. Swarnkar and R. Gopal, *Appl. Surf. Sci.*, 2011, **257**, 9846.
- 76 M. A. P. Almeida, L. S. Cavalcante, J. A. Varela, M. S. Li and E. Longo, *Adv. Powder Technol.*, 2012, **23**, 124.
- 77 L. S. Cavalcante, J. C. Sczancoski, M. S. Li, E. Longo and J. A. Varela, *Colloids Surf., A*, 2012, **396**, 346.
- 78 M. R. D. Bomio, R. L. Tranquilin, F. V. Motta, C. A. Paskocimas, R. M. Nascimento, L. Gracia, J. Andres and E. Longo, *J. Phys. Chem. C*, 2013, **117**, 21382.
- 79 V. K. Lamer and R. H. Dinegar, *J. Am. Chem. Soc.*, 1950, **72**, 4847.
- 80 C. R. A. Catlow, S. T. Bromley, S. Hamad, M. Mora-Fonz, 10 A. A. Sokol and S. M. Woodley, *Phys. Chem. Chem. Phys.*, 2010, **12**, 786.
- 81 D. L. Golic, Z. Brankovic, N. Daneu, S. Bernik and G. Brankovic, *J. Sol-Gel Sci. Technol.*, 2012, **63**, 116.
- 82 J. A. Tossell and D. J. Vaughan, *Geochim. Cosmochim. Acta*, 15 1993, **57**, 1935.
- 83 A. Burnin, E. Sanville and J. J. BelBruno, *J. Phys. Chem. A*, 2005, **109**, 5026.
- 84 J. M. Azpiroz, X. Lopez, J. M. Ugalde and I. Infante, *J. Phys. Chem. C*, 2012, **116**(4), 2740. 20
- 85 M. Zwijnenburg, F. Illas and S. T. Bromley, *Phys. Chem. Chem. Phys.*, 2011, **13**, 9311.
- 86 J. M. Azpiroz, E. Mosconi and F. De Angelis, *J. Phys. Chem. C*, 2011, **115**, 25219.
- 87 M. Zwijnenburg, C. Sousa, F. Illas and S. T. Bromley, 25 *J. Chem. Phys.*, 2011, **134**, 064511.
- 88 J. M. Azpiroz, J. M. Ugalde and I. Infante, *J. Chem. Theory Comput.*, 2014, **10**, 76.
- 89 Y. R. Wang and C. B. Duke, *Phys. Rev. B: Condens. Matter Mater. Phys.*, 1987, **36**, 2763.
- 90 C. Y. Yeh, Z. W. Lu, S. Froyen and A. Zunger, *Phys. Rev. B: Condens. Matter Mater. Phys.*, 1992, **46**, 10086. 30
- 91 T. A. Koopmans, *Physica*, 1933, **1**, 104.

35

35

40

40

45

45

50

50

55

55